Adaptive Control of a MEMS Steering Mirror for Free-space Laser Communications

Néstor O. Pérez Arancibia, Neil Chen, Steve Gibson and Tsu-Chin Tsao

Mechanical and Aerospace Engineering
University of California, Los Angeles 90095-1597

ABSTRACT

This paper presents an adaptive control scheme for laser-beam steering by a two-axis MEMS tilt mirror used in current free-space optical communications systems. In the control scheme presented here, disturbances in the laser beam are rejected by a high-performance linear time-invariant feedback controller augmented by the adaptive control loop, which determines control gains that are optimal for the current disturbance acting on the laser beam. The variable-order adaptive control loop is based on an adaptive lattice filter that implicitly identifies the disturbance statistics from real-time sensor data. Experimental results are presented to demonstrate the effectiveness of the adaptive controller for rejecting multi-bandwidth jitter. These results demonstrate that the adaptive loop significantly extends the jitter-rejection bandwidth achieved by the feedback controller alone.

Keywords: Adaptive control, laser-beam steering, jitter, MEMS mirror, free-space laser communications

1. INTRODUCTION

The developing technology of free-space laser communications demands precise pointing of laser beams and high-bandwidth rejection of disturbances produced by platform vibrations and atmospheric turbulence. Vibration-induced jitter typically is composed of one or more narrow bandwidths produced by vibration modes of the structure supporting the optical system, while turbulence-induced jitter may be rather broadband.[1,2] Also, some fast steering mirrors have lightly damped elastic modes that produce beam jitter. This is the case with the MEMS mirror used to steer the beam in the research described here. These mirrors, which are used in current free-space optical communications systems, have a torsional vibration mode about each steering axis.

Because the disturbance characteristics often change with time, optimal performance of a beam steering system requires an adaptive control system. Recent research on jitter control has produced adaptive control methods that employ least-mean-square (LMS)[3] adaptive filtering and recursive least-squares (RLS) adaptive filtering.[4–6] The trade off is between a simpler algorithm (hence computational economy) with LMS versus faster convergence and exact minimum-variance steady-state performance with RLS.

This paper employs a recursive least-squares lattice filter in the adaptive controller, and introduces a variable-order adaptive control scheme that exploits the order-recursive structure of the lattice filter. The capability to vary the order of the filter in the adaptive controller is important because optimal gains can be identified faster for lower-order filters while higher-order filters are required for optimal steady-state rejection of broadband disturbance. Thus, low filter orders can be used initially for fast adaptation without undesirable transient responses, and the filter order can be increased incrementally to achieve optimal steady-state jitter rejection.

The experiment used for this paper is similar to that used for two previous papers by the authors,[5,6] except for one significant addition. As in these previous papers, a second mirror is used to add jitter to the laser beam; however, in the experiment described here, the MEMS mirror used as the control actuator is mounted on a shaker that vibrates with multiple bandwidths. Thus, there are two jitter sources here, as opposed to one in the authors' previous papers.

Section 2 describes the experimental hardware and configuration. Section 3 describes the system identification of the mirror dynamics and transfer functions require for control system design. Section 4 describes the design of the control system, which consists of a linear time-invariant (LTI) feedback control loop augmented by the adaptive control loop. Experimental results for an experiment with multiple jitter bandwidths are presented in Section 5.

E-mail: nestor@seas.ucla.edu, neilchen@ucla.edu, gibson@ucla.edu, ttsao@seas.ucla.edu

Free-Space Laser Communications V, edited by David G. Voelz, Jennifer C. Ricklin, Proc. of SPIE Vol. 5892
(SPIE, Bellingham, WA, 2005) · 0277-786X/05/$15 · doi: 10.1117/12.619586

Downloaded From: http://journals.spiedigitallibrary.org/ on 03/09/2014 Terms of Use: http://spiedl.org/terms

2. DESCRIPTION OF THE EXPERIMENT

Fig. 1 shows a diagram of the experiment, including the path of the laser beam from the source to the position sensor. The main optical components in the experiment are the laser source, two Texas Instruments MEMS fast steering mirrors, and an On-Trak position sensing device. These components are shown in the photographs in Figs. 2–refontrack. As indicated in Fig. 1, the laser beam leaves the fixed source and reflects first off the mirror FSM 1, which serves as the control actuator. The beam then reflects off the mirror FSM 2, which adds disturbance to the beam direction, and finally goes to the sensor. A lens between FSM 1 and FSM 2 and another lens between FSM 2 and the sensor focus the beam to maintain small spots on FSM 2 and the sensor. There are two sources of jitter in the experiment: the shaker on which the control actuator is mounted and the disturbance actuator FSM 2. The motion of the shaker is vertical, and FSM 2 adds jitter on both mirror axes.

Each mirror rotates about vertical and horizontal axes, denoted by Axis 1 and Axis 2, respectively. The outputs of the sensor are the horizontal and vertical displacements of the centroid of the laser spot on the plane of the On-Track optical sensor. The sensor axes are labeled Axis 1 and Axis 2, respectively, to correspond to beam deflections produced by the mirror rotations. Thus, in the sensor plane, Axis 1 and Axis 2 are horizontal and vertical, respectively.

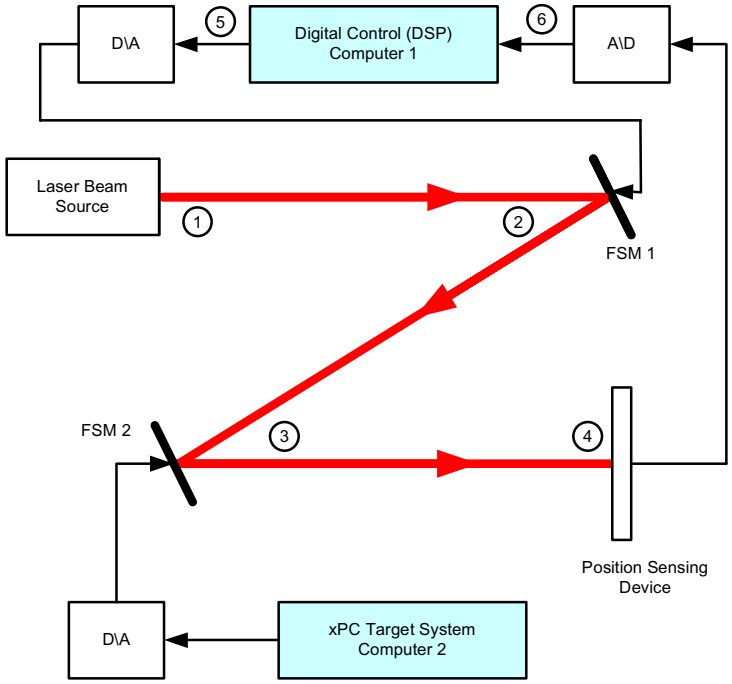

Figure 1. Diagram of the UCLA beam steering experiment. MEMS mirror FSM 1: control actuator mounted on shaker; MEMS mirror FSM 2: disturbance actuator.

The output error in the control problem is the pair of sensor measurements, which are the coordinates of the laser beam spot on the sensor. These measurements, in the form of voltages, go to Computer 1, which has a Texas Instruments TMS320C6701 digital signal processor. This DSP runs both feedback and adaptive controllers and sends actuator commands to FSM 1. Computer 2, a PC running xPC Target, sends disturbance commands to FSM 2. It should be noted that the only measurements used by the adaptive and feedback controllers are the two signals from the On-Trak sensor. The MEMS steering mirror used here has internal optical sensors that supply local measurements of the mirror position, but these measurements were not used in the experiments discussed in this paper.

The commanded rotations of the fast steering mirrors are produced by electromagnetic fields with opposing directions. These fields are created by coils with currents commanded by the control and disturbance computers.

Downloaded From: http://journals.spiedigitallibrary.org/ on 03/09/2014 Terms of Use: http://spiedl.org/terms

The mirrors have a rotation range of ±5 degrees. The reflecting area of the mirrors is 9mm^2. The optoelectronic position sensor at the end of the beam path generates two analog output voltages proportional to the two-dimensional position of the laser beam centroid. In the sensor, quad photo detectors capture the light intensity distribution, generating current outputs, which are converted to voltage and amplified by an operational amplifier. Further electronic processing of these voltage signals yields two final signals, which are the estimates of the centroid coordinates independent of light intensity.

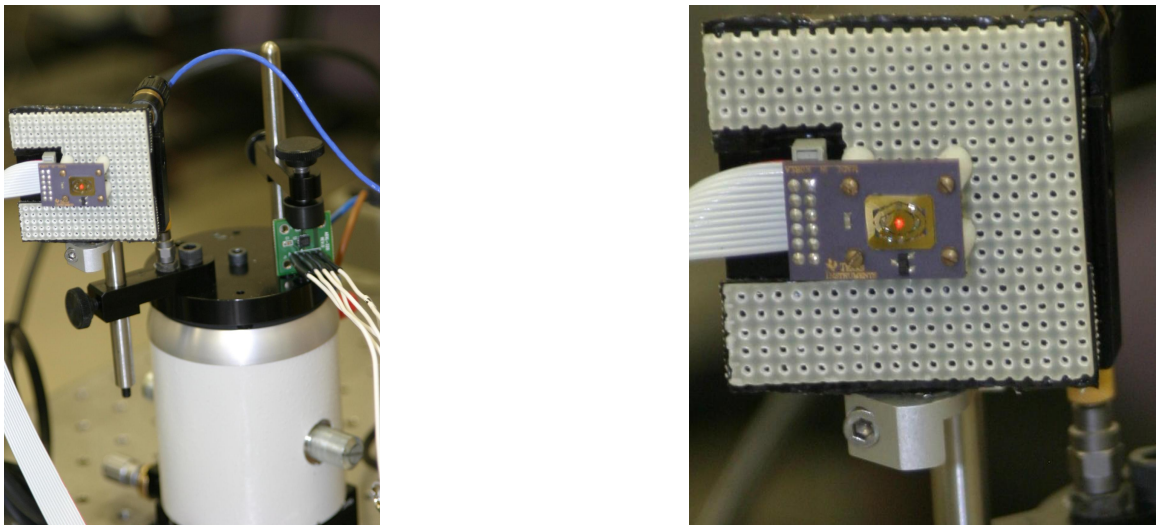

Figure 2. The MEMS fast steering mirror FSM 1 is mounted on the shaker shown at left.

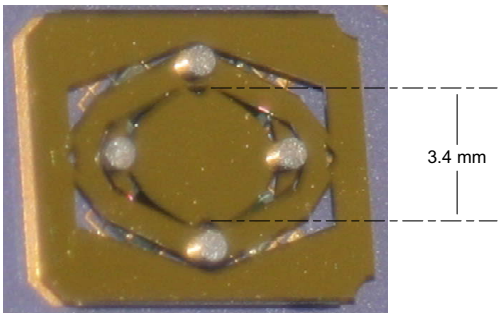

Figure 3. Texas Instruments TALP1000A MEMS fast steering mirror (3.2 mm × 3.6 mm elliptical mirror). Axis 1: vertical; Axis 2: horizontal.

Figure 4. On-Trak Optical Position Sensor. Axis 1: horizontal; Axis 2: vertical. Control objective: maintain red laser spot at center of sensor.

3. SYSTEM IDENTIFICATION

Design of the feedback control system requires an open-loop model of the dynamics of the steering mirror FSM 1, and the adaptive control loop requires an estimate of the transfer function from the adaptive-control commands to the sensor outputs with the feedback loop closed. The open-loop and closed-loop transfer functions are identified by a subspace method[7, 8] using input-output data from two brief experiments in which FSM 1 was driven by

Downloaded From: http://journals.spiedigitallibrary.org/ on 03/09/2014 Terms of Use: http://spiedl.org/terms

white noise. After the first of these experiments, which was open-loop, the feedback controller was designed, and then the feedback loop was closed for the second experiment.

Since the sample-and-hold rate for control and filtering was 2000Hz for the experimental results presented in this paper, discrete-time models were identified for the 2000Hz rate. For identification, input-output sequences with 12,000 data points each (i.e., six seconds of data) were generated.

The disturbance actuator FSM 2 has dynamics very similar to those of FSM 1, but the control loops do not require a model of the disturbance actuator. Hence, the system identification uses data generated with FSM 2 fixed.

Experimental results showed negligible coupling between the two channels of each fast steering mirror; i.e., Axis 1 commands produced negligible rotation about Axis 2 and vice versa. Therefore, an uncoupled pair of SISO transfer functions was identified for the open-loop model of FSM 1. The subspace method identified several higher-order mirror modes, but their contribution to the input-output properties of the mirror were deemed insignificant for the purposes of the control. Therefore, a balanced truncation to two states for each mirror axis was chosen for control purposes. The frequency responses of these identified transfer functions are shown in Fig. 5. The true open-loop transfer function from the FSM 1 commands to the sensor outputs (i.e., the open-loop plant) will be denoted by $P(z)$, and the identified open-loop plant model will be denoted by $\hat{P}(z)$.

As discussed in Section 4, the feedback controller did not couple the mirror modes, so a second uncoupled pair of SISO transfer functions was identified with the feedback loop closed and used by the adaptive control loop. The true closed-loop transfer function and identified closed-loop transfer function will be denoted, respectively, by $G(z)$ and $\hat{G}(z)$. The frequency response of $\hat{G}(z)$ is shown in Fig. 6.

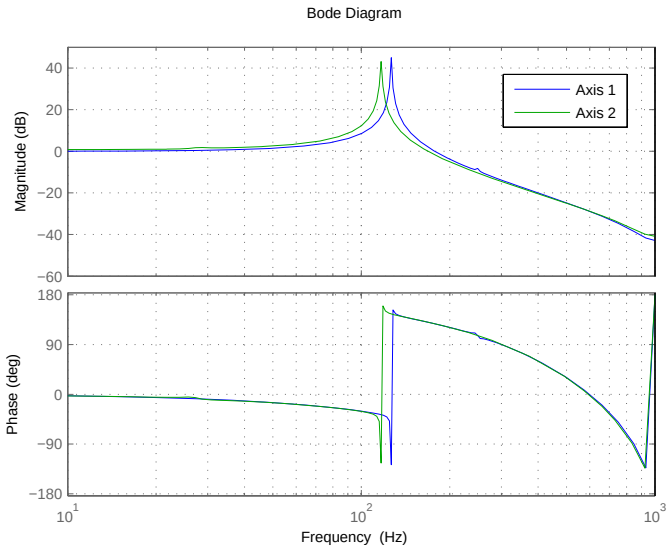

Figure 5. Bode plots for identified model $\hat{P}(z)$ of open-loop fast steering mirror FSM 1 (control actuator). Natural frequencies: 126.5Hz (Axis 1), 116.8Hz (Axis 2).

4. CONTROL DESIGN

In the control scheme for laser beam steering presented here, a linear time-invariant (LTI) feedback control loop is augmented by an adaptive control loop. The LTI feedback loop is a μ-synthesis controller designed to achieve two objectives: a disturbance-rejection bandwidth near the maximum achievable with LTI feedback control, and robust stabilization of the beam steering system. In the adaptive loop, a multichannel RLS lattice filter implicitly identifies the disturbance statistics in real time. The lattice filter was chosen because of its computational efficiency, numerical stability, and order-recursive structure.

Downloaded From: http://journals.spiedigitallibrary.org/ on 03/09/2014 Terms of Use: http://spiedl.org/terms

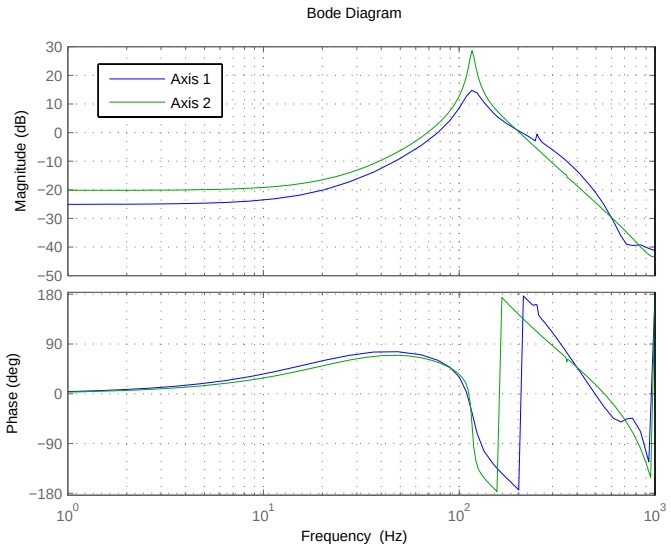

Figure 6. Bode plots for identified transfer function $\hat{G}(z)$ of fast steering mirror FSM 1 with LTI feedback loop closed.

4.1. LTI Feedback Loop

The LTI feedback system is shown in Fig. 7, where $P(z)$ is the open-loop plant and $C(z)$ is a μ-synthesis controller with four states for Axis 1 and six states for Axis 2. The input u in Fig. 7 is the pair of adaptive control commands, and the output y is the pair of beam displacements measured by the sensor. A four-state μ-synthesis controller was designed for each axis.

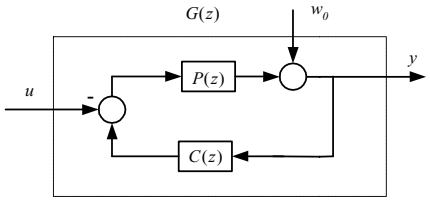

Figure 7. Block diagram of LTI feedback control system. $P(z)$ = open-loop plant; $C(z)$ = μ-synthesis LTI feedback controller; $G(z) = y/u$.

The discrete-time μ-synthesis method was used to design the feedback controller $C(z)$ to reject the noise w_0 in Fig. 7. This design was based on Fig. 8, where Δ represents the plant uncertainty, and $W_U(z)$ and $W_P(z)$ are the uncertainty and performance weighting filters employed in the design. The μ-synthesis design method uses μ-analysis of robust stability and performance to refine iteratively an H_∞ controller. The D-K iteration in the MATLAB μ-Analysis and Synthesis toolbox[9] was used. Also, the guidelines and insights for μ-synthesis design presented in Kim and Tsao[10] were followed to maximize the bandwidth of the closed-loop sensitivity function while maintaining robust stability. The uncertainty and performance weighting filters were

$$W_U = \frac{0.8280z - 0.6787}{z - 0.0045} \tag{1}$$

$$W_P = \frac{0.0083z^2 + 0.0165z + 0.0083}{z^2 - 1.8373z + 0.8439}\,. \tag{2}$$

Fig. 9 shows the two-channel sensitivity transfer function for the modeled beam steering system with the LTI feedback loop closed. The input for this transfer function is a pair of output disturbances represented by

Downloaded From: http://journals.spiedigitallibrary.org/ on 03/09/2014 Terms of Use: http://spiedl.org/terms

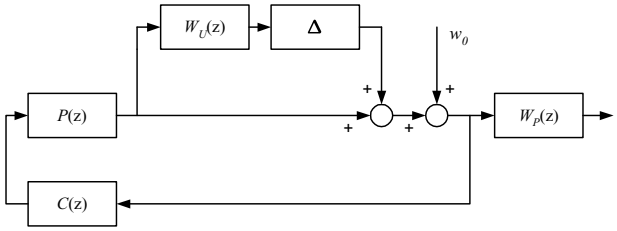

Figure 8. Block diagram for μ-synthesis design of LTI feedback controller.

the signal w_0 in Fig. 7, and the output is the pair of measured beam displacements represented by the signal y in Fig. 7. This sensitivity transfer function was computed using the identified open-loop plant model and the μ-synthesis feedback controller, *without* the adaptive controller. The performance of the LTI feedback loop in the experiment indicates that the transfer function in Fig. 9 closely approximates the true sensitivity transfer function $[I - P(z)C(z)]^{-1}$.

The feedback controller here was designed to maximize the steady-state disturbance-rejection bandwidth, so that there is some associated amplification of higher-frequency disturbance. This trade off is common in high-performance controllers. The high-frequency amplification can be avoided by accepting less disturbance-rejection below 100Hz, but a primary purpose of this paper is to demonstrate how the adaptive controller effectively extends the bandwidth of even a high-bandwidth LTI feedback controller.

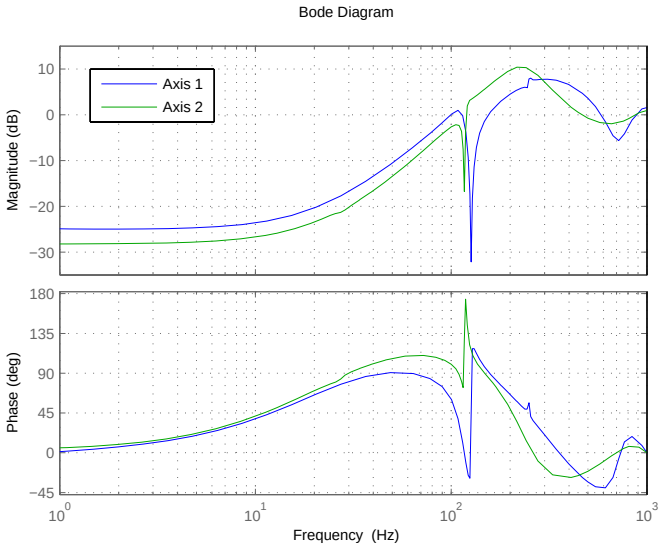

Figure 9. Bode plots for the sensitivity transfer function $[I - \hat{P}(z)C(z)]^{-1}$. Zeros: 126.5Hz (Axis 1), 116.8Hz (Axis 2).

Although maximizing the bandwidth of the closed-loop sensitivity function was the main objective in designing the LTI feedback controller, a good design should stabilize the lightly damped elastic mode associated with each mirror axis. Fig. 6 shows that the feedback controller dampens the natural mode for Axis 1 very effectively, reducing the peak by about 30dB from that in Fig. 5. However, the feedback controller dampens the natural mode for Axis 2 less, reducing the peak by only about 12dB from that in Fig. 5.

The possible reasons for the poorer performance of LTI feedback loop for Axis 2 include poor identification of the Axis 2 transfer function, nonlinear actuator dynamics, and poor convergence of the D-K iteration in the μ-synthesis design process. It is possible to provide more damping to the Axis 2 mode with different control designs, even a relatively simple PID feedback, but only at the expense of a lower disturbance-rejection

Downloaded From: http://journals.spiedigitallibrary.org/ on 03/09/2014 Terms of Use: http://spiedl.org/terms

bandwidth. However, the current feedback controller allows this paper to illustrate the performance of the adaptive loop when one axis is stabilized very well by the LTI feedback loop but one axis is not stabilized as well.

4.2. Adaptive Control Loop

In typical beam-steering applications, including adaptive optics and optical wireless communications, the dynamic models of the fast steering mirrors either are known or can be determined by a one-time identification as in Section 3. The disturbance characteristics, however, depend on the atmospheric conditions in the optical paths and on the excited vibration modes of the structures on which the optical systems are mounted, so that the disturbance characteristics commonly vary during operation of a beam steering system. Therefore, the adaptive control algorithm presented in this paper assumes known LTI plant dynamics but unknown disturbance dynamics. The adaptive controller requires an estimate $\hat{G}(z)$ of the closed-loop transfer function $G(z)$ in Fig. 7. The RLS lattice filter in the adaptive control loop tracks the statistics of the disturbance and identifies gains to minimize the RMS value of the beam displacement.

The adaptive control scheme used here is similar to the adaptive control schemes used in Kim et al.[4] for experimental adaptive control of a different type of fast steering mirror with much lower bandwidth than the MEMS mirror here, and in recent papers on adaptive optics[11–14] where many sensor and control channels were used but with lower filter orders than used here. The main control-scheme innovation in this paper is the variable-order nature of the adaptive controller.

Fig. 10 shows the structure of the adaptive control loop. The disturbance signal w in Fig. 10 is related to the disturbance signal w_0 in Fig. 7 by the sensitivity transfer function produced by the LTI feedback loop (see Fig. 9):

$$w = [I - P(z)C(z)]^{-1} w_0 \, . \tag{3}$$

The adaptive FIR filter $F(z)$ is the main component of the adaptive controller. As shown in Fig. 10, the adaptive controller uses two copies of the FIR filter. The optimal filter gains are estimated in the bottom part of the block diagram in Fig. 10, and these gains are used by the FIR filter in the top part of Fig. 10 to generate the adaptive control signal u..

For the results presented in this paper, the two channels of the adaptive controller were uncoupled, although the adaptive lattice filter permits the use of multiple sensor channels for generating the command for each control channel. Comparison of a variety experimental results for the jitter-control system here showed that coupling the two channels in the adaptive controller produced no improvement in steady-state performance but the FIR gains converged faster to the optimal values for the uncoupled case because this case involves fewer FIR gains. Because of the multichannel nature of the lattice filter, the adaptive control algorithm can accommodate additional sensor signals, such as accelerometer measurements.

The lattice structure of the FIR filter that generates the adaptive control commands is illustrated in Fig. 11. The lattice realization of an FIR filter of order N consists of N identical stages cascaded as in Fig. 11. The details of the lattice-filter algorithms represented by the blocks in Fig. 11 are beyond the scope of this paper. These algorithms are reparameterized versions of algorithms in Jiang and Gibson.[15] The current parameterization of the lattice algorithms is optimized for indefinite real-time operation. The current lattice filter maintains two important characteristics of the RLS lattice filter in Jiang and Gibson[15]: channel orthogonalization, which is essential to numerical stability in multichannel applications, and the unwindowed property of the lattice filter, which is essential to rapid convergence.

As indicated in Fig. 11, each stage of the lattice filter generates an adaptive control command. For $n \geq 1$, the output u_n from the n^{th} stage is the optimal control command if an FIR filter of order n is used in the adaptive control loop. For hardware implementation, a maximum filter order N is selected. In each real-time sampling interval, the lattice filter generates the adaptive control commands for all filter orders from 1 to N, and the control algorithm can select which command to use.

Downloaded From: http://journals.spiedigitallibrary.org/ on 03/09/2014 Terms of Use: http://spiedl.org/terms

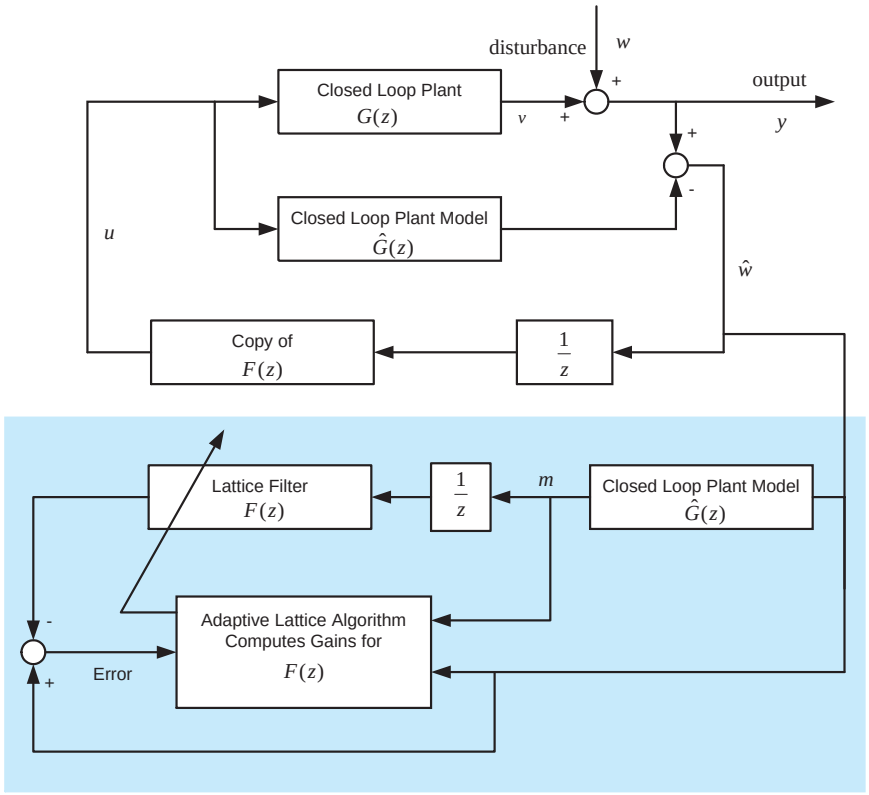

Figure 10. Block diagram of adaptive control system.

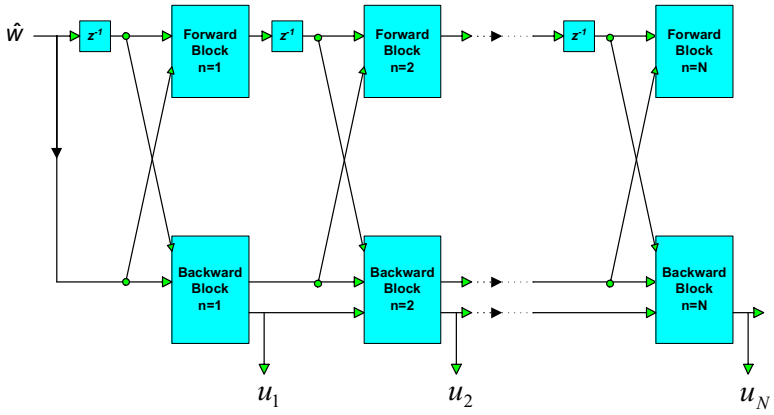

Figure 11. The FIR lattice filter generates adaptive control commands u_k for all filter orders $k \leq N$.

It should be emphasized that, because of the order-recursive structure of the lattice filter, computing the control commands for all orders from 1 to N requires no more computation than computing the control command for the order N alone. It appears that lattice filters are the only RLS algorithms with this property. Therefore, lattice filters are uniquely suited to variable-order adaptive control.

The capability to vary the order of the filter in the adaptive controller is important because optimal gains can be identified faster for lower-order filters while higher-order filters are required for optimal steady-state rejection of broadband disturbance. When the adaptive control loop is first closed or when it is adapting to changing

Downloaded From: http://journals.spiedigitallibrary.org/ on 03/09/2014 Terms of Use: http://spiedl.org/terms

disturbance statistics, lower-order control commands should be used initially. The order of the control commands can be increased incrementally as the gains for the higher-order filter stages converge. This procedure eliminates large transient responses often produced by initially incorrect gains in high-order filters.

5. EXPERIMENTAL RESULTS

In the experiments described here, the sample-and-hold rate for control and filtering was 2000Hz. Computer 2 in Fig. 1 sent jitter command sequences of multiple bandwidths to both the disturbance mirror FSM 2 and the shaker. The same command sequence was sent to both axes of FSM 2. The command sequence sent to the shaker was the sum of the command sequence sent to FSM 2 and five sine waves (i.e., five discrete frequencies). These bandwidths and discrete frequencies were

$$\begin{aligned} \text{jitter bandwidths for FSM 2 and shaker} &= \text{10Hz–20Hz, 190Hz–200Hz, 350–360Hz} \\ \text{frequencies of sine waves for shaker} &= \text{15Hz, 40Hz, 125Hz, 195Hz, 355Hz.} \end{aligned} \tag{4}$$

Figs. 12 and 13 compare the errors (i.e., coordinates of the laser spot on the position sensor) of the beam position on the sensor for three cases: (1) open-loop, (2) LTI feedback control only, (3) LTI feedback control augmented by adaptive control. Fig. 12 shows the time series for five-second's worth of data (10,000 samples), and Fig. 13 shows the corresponding power spectral densities for the last 2.5 seconds (5000 samples) of each time series. The open-loop errors are the jitter sequences added to the laser beam by the disturbance mirror FSM 2 and the shaker.

When the adaptive controller was used, the RLS lattice filter began running after the time labeled 2 sec in the bottom time-series plots in Fig. 12, but no adaptive control commands were sent to the control actuator FSM 1 until 50 time steps later. Thus, the adaptive filter had 50 initial training steps to obtain initial estimates of the FIR gains before the adaptive control loop was closed at 2.025 sec. It should be emphasized that, when the lattice filter began running at two seconds, it had no initial information about the statistics of the jitter or estimates of the FIR gains.

Fig. 14 shows how the order of the FIR lattice filter generating the control commands changed with time. The initial FIR order was $n = 4$, and the order was incremented by 4 at the end of 50-step intervals until it reached the maximum FIR order $N = 16$ at one second plus 200 steps, or 2.1 sec. Thus, the FIR order used for control reached its maximum at 0.1 sec after the lattice filter began running with no initial information about the disturbance statistics. For these and other similar experiments, the performance of the adaptive loop was evaluated with several maximum lattice-filter orders. The order 16 yielded better steady-state performance than lower orders, but orders higher than 16 yielded no significant further improvement. In both experiments and simulations, the variable-order property of the adaptive controller has proved essential for eliminating large initial transients that sometimes occur when a fixed-order adaptive control loop is closed.

The time series in Fig. 12 show rapid convergence to optimal steady-state performance, which this adaptive control algorithm has produced consistently in experiments. For the experiment presented here, the adaptive controller achieves near optimal jitter rejection in about 0.25 sec, or 500 samples, and the adaptive controller achieves significant reduction in the output error within 0.1 sec.

The PSDs in Fig. 13 show that, as predicted by Fig. 9, the LTI feedback loop significantly reduces jitter below about 75Hz but generally amplifies jitter above about 150Hz. The LTI feedback loop also reduces the PSD magnitude between 125Hz and 140Hz for Axis 1, and in the vicinity of 117Hz for Axis 2. These two reductions agree with the zeros of the sensitivity transfer function in Fig. 9, which result from the open-loop natural frequencies of FSM 1. The small peak at 126.5Hz in the open-loop PSD for Axis 1 and the large peak at 116.8Hz in the open-loop PSD for Axis 2 also result from the modes of FSM 1, which are excited by the shaker.

The PSDs show that the adaptive loop yields significant jitter reduction above 75Hz, thereby extending the bandwidth of the feedback loop. This extended bandwidth accounts for the significant reduction in the amplitudes of the output errors achieved by the adaptive controller, as shown in Fig. 12.

Downloaded From: http://journals.spiedigitallibrary.org/ on 03/09/2014 Terms of Use: http://spiedl.org/terms

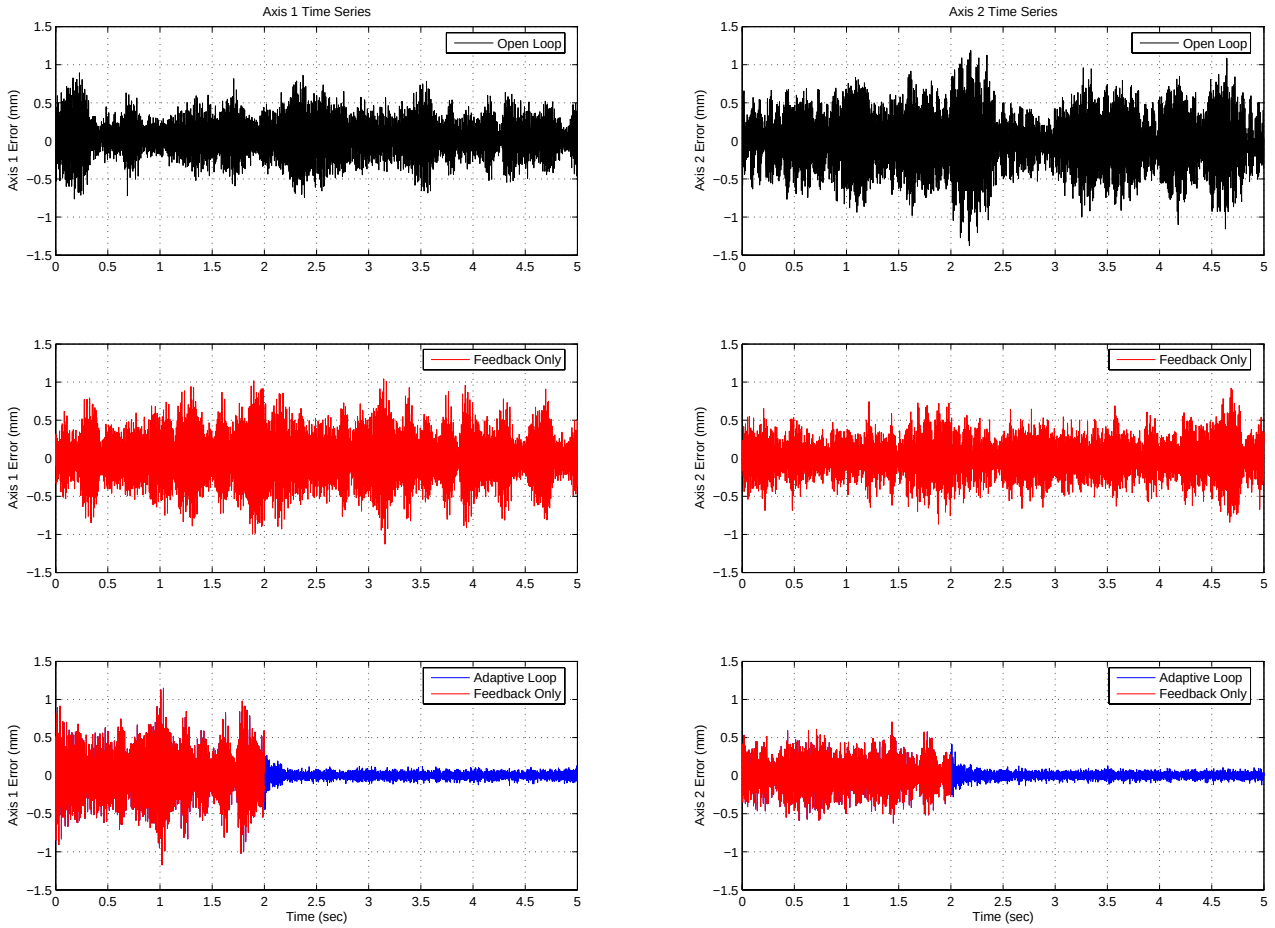

Figure 12. Output-error time series. *Top:* open loop; *middle:* LTI feedback control only; *bottom:* LTI feedback control augmented by variable-order adaptive control. *Left:* Axis 1. *Right:* Axis 2. Lattice filter started running at 2 sec; adaptive control loop was closed at 2.025 sec.

Another noteworthy point in the PSDs in Fig. 13 is that, while both the feedback loop and the adaptive loop amplify low-power jitter above 150Hz, the high-frequency amplification often is greater for the adaptive loop—but only at frequencies where there is very little jitter. The explicit objective of the RLS lattice filter is to minimize the RMS values of the output error, and this is accomplished. As is well known, filters and controllers that minimize the RMS values of error signals tend to whiten residual errors, so that optimum filters and controllers typically accept some amplification in frequency bands where the disturbance is very low to be able to achieve large reductions in the dominant disturbance power. This is true for minimum-variance LTI feedback controllers as well as for high- performance adaptive controllers like the one used here. As the time series show, the jitter in bandwidths with low power is not amplified enough to make it significant.

Downloaded From: http://journals.spiedigitallibrary.org/ on 03/09/2014 Terms of Use: http://spiedl.org/terms

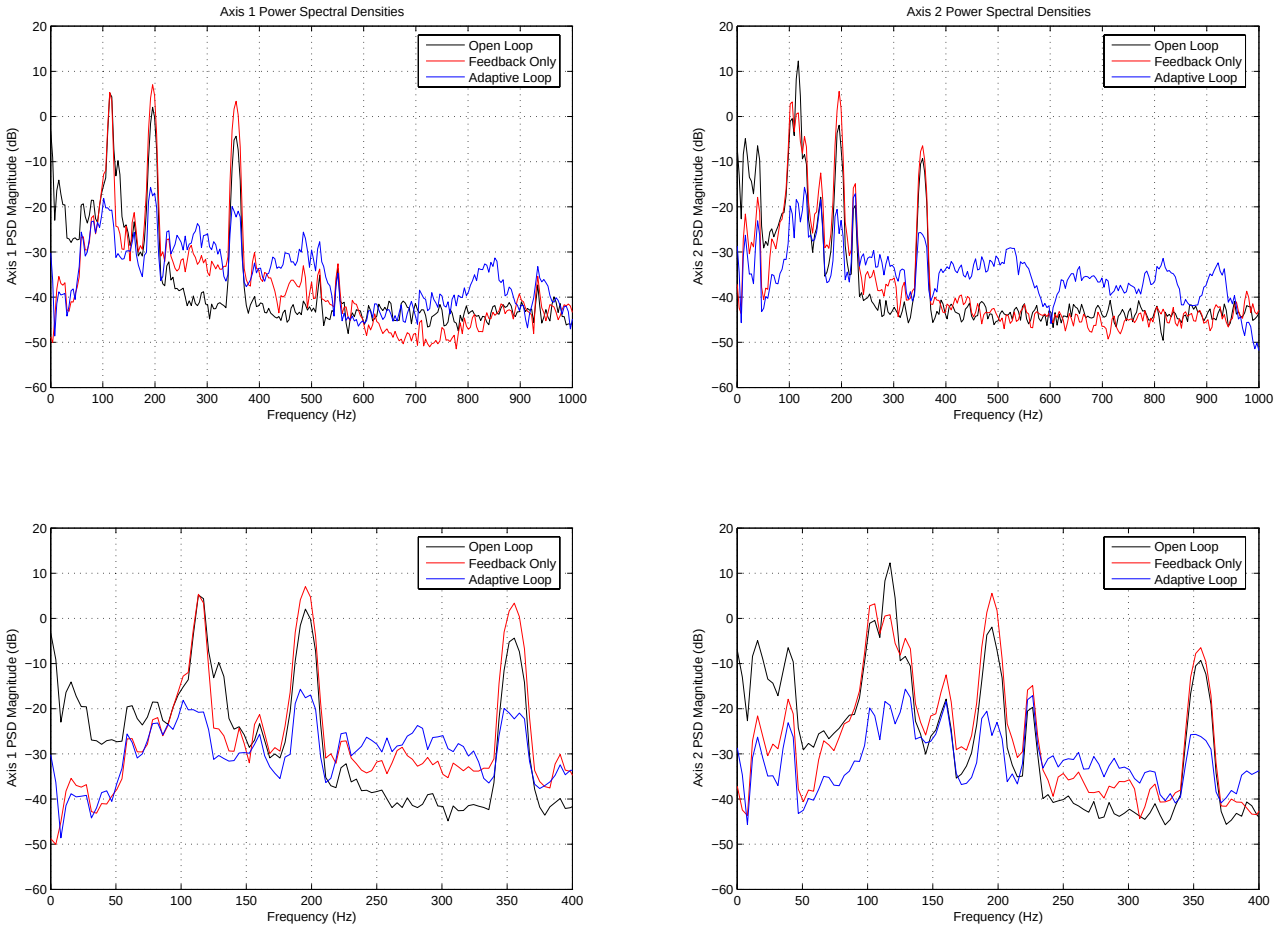

Figure 13. Output-error power spectral densities for open loop, LTI feedback only, and LTI feedback augmented by adaptive control. PSDs computed for last 2.5 seconds (5000 samples). *Bottom:* Zoomed view from top.

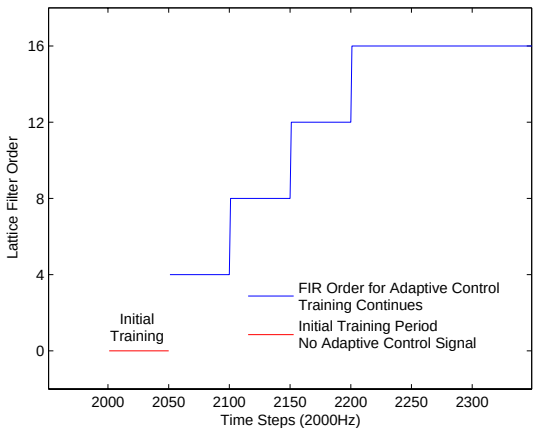

Figure 14. Order of the FIR lattice filter that generated the variable-order adaptive control signal. At the beginning of the initial training period, the lattice filter had no initial information about the statistics of the jitter or estimates of the FIR gains. The adaptive control loop was closed with FIR order $n = 4$ after the 50-step initial training period.

Downloaded From: http://journals.spiedigitallibrary.org/ on 03/09/2014 Terms of Use: http://spiedl.org/terms

6. CONCLUSIONS

This paper has presented a new method for adaptive control of jitter in laser beams. The method has been demonstrated by results from an experiment employing two-axis MEMS tilt mirrors. Laser beam jitter is rejected by a μ-synthesis feedback controller augmented by a variable-order adaptive controller, which determines control gains that are optimal for the current disturbance acting on the laser beam. The adaptive loop is based on an RLS lattice filter that implicitly identifies the disturbance statistics from real-time sensor data. Experimental results demonstrate that the adaptive controller significantly extends the disturbance rejection bandwidth achieved by the feedback controller alone. The adaptive lattice filter can perform high order, multi-channel RLS (recursive-least-squares) computation in real-time at high sampling rates, and the RLS algorithm yields faster convergence to optimal gains than does the LMS method, which is used more commonly in adaptive disturbance-rejection applications. Even though a robust, high-performance feedback controller is used here, the experimental results demonstrate that the adaptive controller greatly extends the jitter-rejection bandwidth.

ACKNOWLEDGMENTS

This work was supported by the U. S. Air Force Office of Scientific Research under AFOSR Grants F49620-02-01-0319 and F-49620-03-1-0234.

REFERENCES

1. M. C. Roggemann and B. Welsh, *Imaging through Turbulence*, CRC, New York, 1996.
2. R. K. Tyson, *Principles of Adaptive Optics*, Academic Press, New York, 1998.
3. Mark A. McEver, Daniel G. Cole, and Robert L. Clark, "Adaptive feedback control of optical jitter using Q-parameterization," *Optical Engineering* , pp. 904–910, April 2004.
4. Byung-Sub Kim, Steve Gibson, and Tsu-Chin Tsao, "Adaptive control of a tilt mirror for laser beam steering," in *American Control Conference*, IEEE, (Boston, MA), June 2004.
5. Néstor O. Pérez Arancibia, Steve Gibson, and Tsu-Chin Tsao, "Adaptive control of MEMS mirrors for beam steering," in *IMECE2004*, ASME, (Anaheim, CA), November 2004.
6. Néstor O. Pérez Arancibia, Neil Chen, Steve Gibson, and Tsu-Chin Tsao, "Adaptive control of a MEMS steering mirror for suppression of laser beam jitter," in *American Control Conference*, IEEE, (Portland, OR), June 2005.
7. Y. M. Ho, G. Xu, and T. Kailath, "Fast identification of state-space models via exploitation of displacement structure," *IEEE Transactions on Automatic Control* **39**, pp. 2004–2017, October 1994.
8. P. Van Overschee and B. De Moor, *Subspace Identification for Linear Systems*, Kluwer Academic Publishers, Norwell, MA, 1996.
9. G. J. Balas, J. C. Doyle, K. Glover, A. Packard, and R. Smith, *μ-Analisis and Synthesis Toolbox*, Mathworks, 1995.
10. B.-S. Kim and T.-C. Tsao, "A performance enhancement scheme for robust repetitive control system," *ASME Journal of Dynamic Systems, Measurement, and Control* **126**, pp. 224–229, March 2004.
11. J. S. Gibson, C.-C. Chang, and B. L. Ellerbroek, "Adaptive optics: wavefront correction by use of adaptive filtering and control," *Applied Optics, Optical Technology and Biomedical Optics* , pp. 2525–2538, June 2000.
12. J. S. Gibson, C.-C. Chang, and Neil Chen, "Adaptive optics with a new modal decomposition of actuator and sensor spaces," in *American Control Conference*, (Arlington, VA), June 2001.
13. Yu-Tai Liu and Steve Gibson, "Adaptive optics with adaptive filtering and control," in *American Control Conference*, IEEE, (Boston, MA), June 2004.
14. Yu-Tai Liu, Neil Chen, and Steve Gibson, "Adaptive filtering and control for wavefront reconstruction and jitter control in adaptive optics," in *American Control Conference*, IEEE, (Portland, OR), June 2005.
15. S.-B. Jiang and J. S. Gibson, "An unwindowed multichannel lattice filter with orthogonal channels," *IEEE Transactions on Signal Processing* **43**, pp. 2831–2842, December 1995.

Downloaded From: http://journals.spiedigitallibrary.org/ on 03/09/2014 Terms of Use: http://spiedl.org/terms